Ralf Frotscher and Manfred Staat*

Stresses produced by different textile mesh implants in a tissue equivalent

Abstract: Two single-incision mini-slings used for treating urinary incontinence in women are compared with respect to the stresses they produce in their surrounding tissue. In an earlier paper we experimentally observed that these implants produce considerably different stress distributions in a muscle tissue equivalent. Here we perform 2D finite element analyses to compare the shear stresses and normal stresses in the tissue equivalent for the two meshes and to investigate their failure behavior. The results clearly show that the Gynecare TVT fails for increasing loads in a zipper-like manner because it gradually debonds from the surrounding tissue. Contrary to that, the tissue at the ends of the DynaMesh-SIS direct may rupture but only at higher loads. The simulation results are in good agreement with the experimental observations thus the computational model helps to interpret the experimental results and provides a tool for qualitative evaluation of mesh implants.

Keywords: finite element analyses; incontinence; orthotropic textile meshes; pelvic floor.

DOI 10.1515/bnm-2014-0003
Received April 16, 2014; accepted July 1, 2014; previously published online August 5, 2014

Introduction

In pelvic floor surgery mesh implants are commonly used to treat urinary incontinence and to repair pelvic organ prolapse. Several single-incision mini-sling systems have been market that are made of meshes with largely different mechanical properties, like dimension, material, the way of knitting, the number of threads used for the knitting, thickness of the threads, pore size and orientation of the pores. Due to the numerous differences, the mesh implants already have been mechanically investigated with respect to all those properties. Uniaxial tension tests, tearing tests, bending burst tests, other loading experiments and image analysis have been conducted to determine maximum forces, strain, stress, pull-out strength, the degree of anisotropy and material parameters, e.g. in [1–5]. As shown in [6], a characterization of the mesh porosity and the deformation state of the pores during loading is of major importance because they have a large influence to tissue inflammation and ingrowing behavior. Further, hysteresis curves for cyclic loading of the meshes have been investigated, e.g. in [7, 8]. Aside from pure experimental testing, finite element models already have been established for a computational investigation of surgical mesh implants and their surrounding tissue, e.g. in [9].

In this paper we compare two different meshes, the Gynecare TVT (GC) of Ethicon (Somerville, USA) and DynaMesh-SIS direct (SD) of FEG Textiltechnik (Aachen, Germany). We choose these meshes because they have a considerably different structure and although designed for the same mission they have principally distinct mechanical characteristics with respect to pull-out behavior and load transfer in the surrounding tissue. All experimental results that we computationally validate and interpret here have been presented in [5]. Therein we present an experimental method for measuring the pull-out strength and visualizing the maximum shear stresses in a muscle tissue equivalent using photoelasticity. The meshes are embedded in a block of ballistic gelatin of 255–265 Bloom Type A (Gelita AG, Germany, product name: Type Ballistic 3) which mimics the mechanical properties of muscle tissue but is transparent and photoelastic. The free end of the mesh has been clamped into a tension machine. At the opposite end of the gelatin block another textile tissue is embedded allowing a clamping of the gelatin block. Applying tension to the mesh with the gelatin block between two polarizing filters leads to isochromatic lines that represent lines of equal maximum shear stresses.

***Corresponding author: Manfred Staat,** Biomechanics Laboratory, Institute of Bioengineering, Aachen University of Applied Sciences, Heinrich-Mußmann-Straße 1, 52428 Jülich, Germany,
Phone: +49 241/6009-53120, Fax: +49 241/6009-53199,
E-mail: m.staat@fh-aachen.de
Ralf Frotscher: Biomechanics Laboratory, Institute of Bioengineering, Aachen University of Applied Sciences, Heinrich-Mußmann-Straße 1, 52428 Jülich, Germany

The maximum shear stress that is observable in photoelasticity is the so-called Tresca stress which is a popular failure criterion for ductile materials like metals failing by slipping in planes which are inclined by 45° against the principal stress directions. Like a brittle material, gelatin fails in tension under maximum normal stress in the plane of the largest principal stress. We assume a similar behavior of soft biological tissue. Therefore we use the finite element method (FEM) to calculate shear stresses for comparison with the experiments and normal stresses as a failure criterion for the soft tissues into which the prosthetic meshes are implanted.

Gynecare and SIS direct

The two investigated meshes are shown in Figures 1 and 2. These two meshes are considerably different with respect to the material, pore shape, knitting and pore orientation. The geometrical properties have been determined using a KEYENCE VHX-600DSO digital microscope (Neu-Isenburg, Germany) and are shown in Table 1.

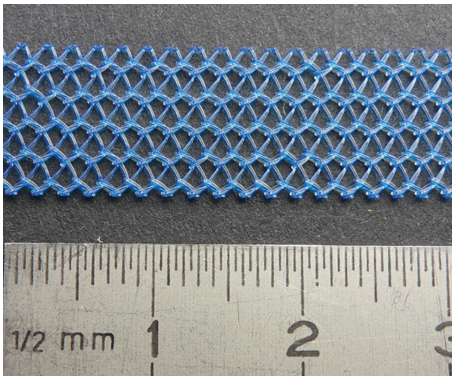

Figure 1 Gynecare, Ethicon (Somerville, USA).

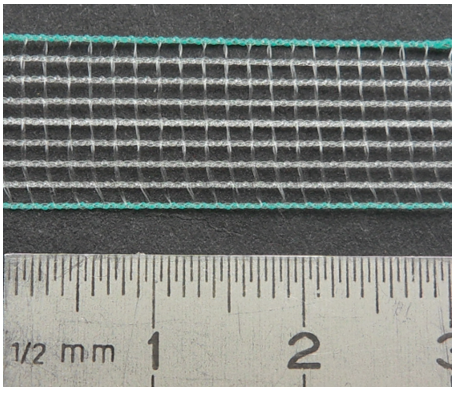

Figure 2 SIS direct, FEG Textiltechnik (Aachen, Germany).

Table 1 Geometrical properties of SD and GC.

Mesh	Pore shape	Pore length	Pore width	Fiber thickness
SIS direct (SD)	Rectangular	≈1.45 mm	≈1.1 mm	≈0.2 mm
Gynecare TVT (GC)	Rhomboidal	≈1.8 mm	≈1.4 mm	≈0.5 mm

Special attention needs to be paid to the thread thickness and the overall structure of the respective mesh. One single thread thickness is difficult to determine because both meshes consist of multiple interwoven threads. In the computational model we represent only a fiber without distinguishing the single threads because of computation time and because we are mostly interested in the structural effects of the respective mesh. The geometrical structure of the GC is more complex than the structure of the SD. The GC consists of rows of rhomboidal pores with alternating orientation, whereas the SD has very simple regular rectangular pores.

Computational model

We geometrically represent both meshes assuming that they consist of one fiber using the geometrical information given in Table 1. Meshes of approximately 75 mm length and 12 mm width are embedded into a gelatin block of 150 mm length and 90 mm width which are the dimensions of the gelatin blocks in the experiments. For the investigation of the shear stresses the length of the meshes is 25 mm for better comparability with experimental results. The thickness direction is not modeled here in order to keep the computational model small. Using the plane stress assumption, discretizing the two-dimensional model with second-order triangular finite elements and applying proper boundary conditions and material information to the model we can simulate different load cases and investigate the normal and shear stress distributions in order to qualitatively investigate the influence of the mesh structure.

From the material point of view we model the gelatin with the hyperelastic Neo-Hookean material. The hyperelastic material parameter C_{10}=0.15 MPa and the Poisson's ratio ν=0.45 have been determined from compression tests and are in accordance with the literature. The meshes are modeled as elastic orthotropic materials with the material parameters given in Table 2. The longitudinal and transversal (horizontal and vertical direction in Figures 1 and 2, respectively) Young's moduli E_L, E_T are taken from [4] for the structurally similar meshes Ultrapro (GC) and Parietex

Table 2 Orthotropic material parameters of the meshes. E_L, E_T and G_{LT} are given in MPa.

Mesh	E_L	E_T	ν_{LT}	G_{LT}
SIS direct	12.26	5.28	0.07	4.37
Gynecare	10.21	0.87	0.65	3.09

(SD) and the in-plane Poisson's ratios ν_{LT} have been determined in [5]. The Poisson's ratio of the GC mesh is larger than 0.5 because of its orthotropic structure.

The uniaxial tension tests not only are physically nonlinear but also geometrically nonlinear. Large displacement occurs in the textile mesh and the gelatin and moreover the gelatin is around ten times softer than the mesh and therefore is largely deformed. Thus this nonlinear problem is solved numerically in a Newton-Raphson scheme taking into account all types of nonlinearity.

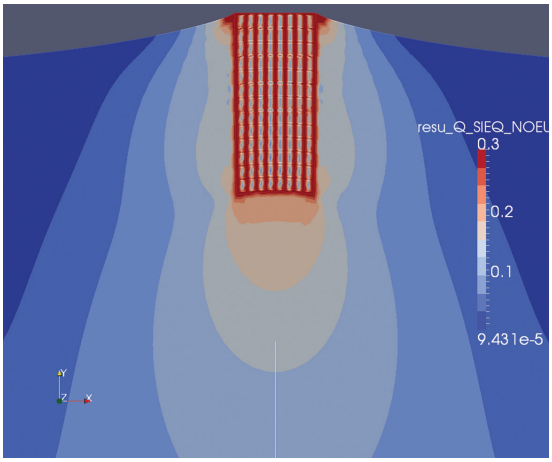

Figure 4 Maximum shear stress in a simulated tension test of the SD mesh embedded in gelatin, τ_{max}=1.79 MPa.

Results

In this section we compare the overall maximum shear stress (Tresca equivalent stress) and the larger principal stress (maximum in-plane normal stress) in the gelatin as it is produced by the two meshes in tension tests. For visual comparability the scale for each stress component is manually chosen in the figures and its actual maximum value is given in the respective caption. The engineering strain in the simulations of the SD mesh is 10%. An equal tensile force is applied in the simulations of the GC mesh, resulting in 10.71% engineering strain. The comparison of the engineering strains reveals that the overall response of the GC mesh is softer than that of the SD mesh.

First we compare the photoelastic experimental results of the SD and the GC meshes with the respective simulated maximum shear stress. Figures 3 and 4 for the SD mesh and Figures 5 and 6 for the GC mesh clearly show that the isochromatic lines in the experimental results are similar to the contour lines of the Tresca equivalent stress in the simulations. There are two major differences one can observe. Firstly there are stress concentrations at

Figure 3 Isochromatic lines in a tension test of the SD mesh embedded in gelatin.

Figure 5 Isochromatic lines in a tension test of the GC mesh embedded in gelatin.

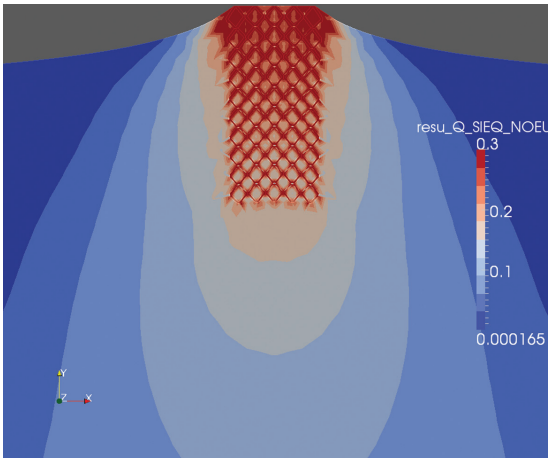

Figure 6 Maximum shear stress in a simulated tension test of the GC mesh embedded in gelatin, τ_{max}=3.58 MPa.

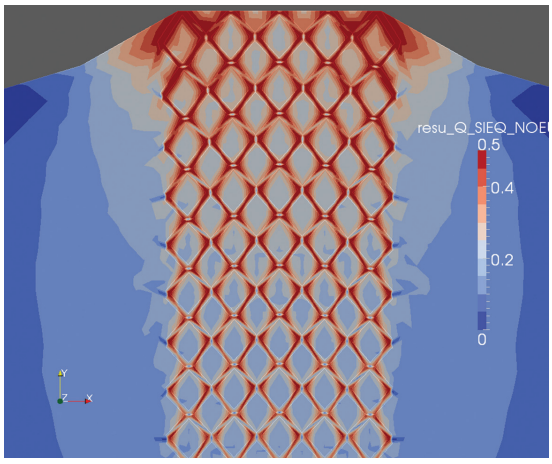

Figure 8 Larger principal stress in the GC mesh simulation, σ_y^{max}=2.75 MPa.

the outer corners at the side of the GC mesh that do not appear at the side of the SD mesh. Secondly the maximum shear stress in the gelatin is two times larger for the GC mesh which becomes apparent from the maximum shear stresses given in the captions.

Interesting observations can be made for the maximum principal stress shown in Figures 7 and 8. In the case of the SD mesh the highest stresses mostly occur in the mesh itself and not in the tissue. On the other hand, the GC mesh produces much larger stress in the gelatin. Especially close to the clamping of the mesh the stress is considerably larger. Again, there are concentrations of the maximum principal stress at the sides of the GC mesh although they appear at the inner corners, contrary to the shear stress concentrations.

Figures 9 and 10 compare the larger principal stress at the unloaded end of both meshes. Obviously the SD mesh

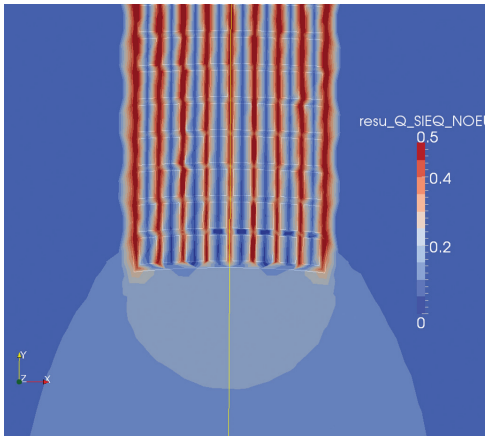

Figure 9 Larger principal stress in the SD mesh simulation, σ_y^{max}=2.57 MPa.

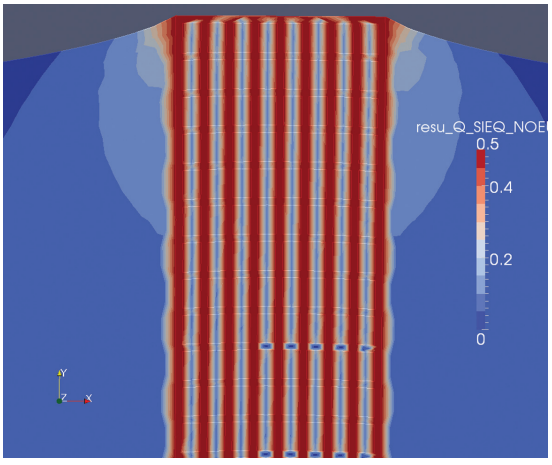

Figure 7 Larger principal stress in the SD mesh simulation, σ_y^{max}=2.57 MPa.

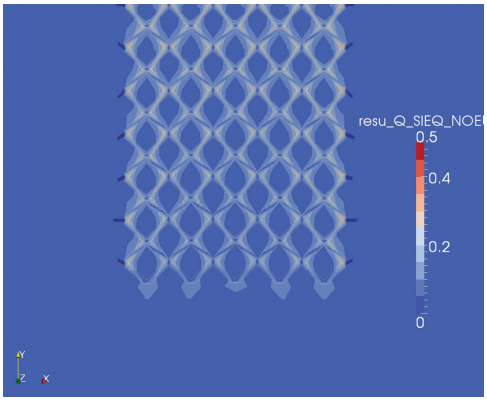

Figure 10 Larger principal stress in the GC mesh simulation, σ_y^{max}=2.75 MPa.

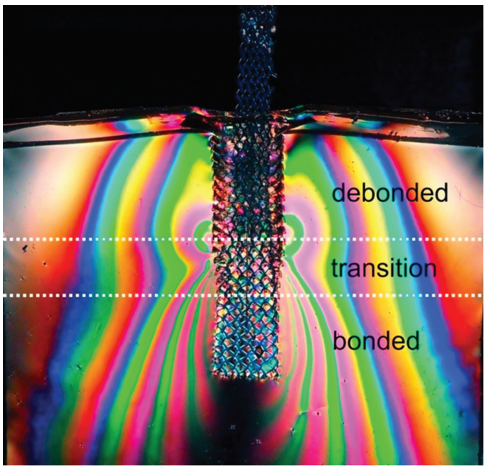

Figure 11 Debonding of the GC mesh from the gelatin.

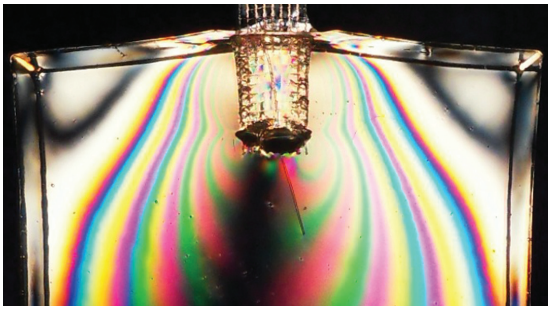

Figure 12 Rupture of the gelatin at the end of the SD mesh.

produces considerably higher stresses in the gelatin at this end compared to the GC mesh.

Conclusion

We observed that both meshes show considerably different stress distributions in the surrounding tissue. The differences do not result from the material itself but from the geometrical structure of the meshes. The SD mesh is quite stiff and therefore the principal stress in the mesh itself is always rather high but more importantly the maximum principal stress in the surrounding tissue is small.

Contrary to that the GC mesh is very flexible due to the rhomboidal structure of its pores. Consequently it does not carry much load resulting in large stresses in the surrounding tissue. Given the large maximum principal stress close to the clamped end of the mesh and compressive and tensile stress concentrations at the inner and outer corners at its sides we can verify an experimental result that is shown in Figure 11. Under tensile load the GC mesh gradually detaches from the gelatin in a zipper-like manner. The closer it is to the clamp, the earlier the region of the mesh will detach from the gelatin because the tensile loading leads to strongly deformed rhomboidal pores that cut through the tissue. The change of pore size and shape that we observed during loading in the debonded section has also been investigated for meshes before ingrowth in [10]. Obviously the porosity of the meshes influences the healing process and scarring and therefore it needs more attention.

On the other hand, the connection between the surrounding tissue and the SD mesh will first fail at the ingrown end of the mesh because of the comparably large normal stresses there. Due to its structure the mesh will not deform much and therefore, if rupture occurs, it will fail immediately. This simulation can be verified by the experimental result shown in Figure 12 where the black region at the ingrown end of the SD mesh indicates a crack-like gap with crack tips which propagate until complete rupture of the gelatin block. Nevertheless, the SD mesh shows a reduced risk of tissue damage when it is loaded by the same tension as the GC mesh.

Acknowledgments: The experiments have been supported by the Federal Ministry of Economics and Technology (BMWi) through the ZIM cooperative project “Einstellbares alloplastisches Schlingensystem zur minimal-invasiven Therapie der Belastungsinkontinenz bei Frauen”. The FEM analyses have been supported by the Federal Ministry of Education and Research (BMBF) through the FHProfUnt project “Optimierung des Systems Netzimplantat-Beckenboden zur therapeutischen Gewebeverstärkung nach der Integraltheorie” (BINGO).

References

1. Krause H, Bennett M, Forwood M, Goh J. Biomechanical properties of raw meshes used in pelvic floor reconstruction. Int Urogynecol J Pel 2008;19:1677–81.
2. Jones KA, Feola A, Meyn L, Abramowitch SD, Moalli PA. Tensile properties of commonly used prolapse meshes. Int Urogynecol J Pel 2009;20:847–53.
3. Deeken CR, Abdo MS, Frisella MM, Matthews BD. Physicomechanical evaluation of polypropylene, polyester, and polytetrafluoroethylene meshes for inguinal hernia repair. J Am Coll Surgeons 2011;212:68–79.
4. Saberski ER, Orenstein SB, Novitsky YW. Anisotropic evaluation of synthetic surgical meshes. Hernia 2011;15:47–52.
5. Staat M, Trenz E, Lohmann P, Frotscher R, Klinge U, Tabaza R, et al. New measurements to compare soft tissue anchoring systems in pelvic floor surgery. J Biomed Mater Res B 2012;4:924–33.

6. Mühl T, Binnebösel M, Klinge U, Goedderz T. New objective measurement to characterize the porosity of textile implants. J Biomed Mater Res B 2008;84:176–83.
7. Röhrnbauer B. Mechanical characterization and modeling of prosthetic meshes. PhD thesis, ETH Zürich, 2013.
8. Röhrnbauer B, Mazza E. Uniaxial and biaxial mechanical characterization of a prosthetic mesh at different length scales. J Mech Behav Biomed 2014;29:7–19.
9. Hernández-Gascón B, Peña E, Melero H, Pascual G, Doblaré M, Ginebra MP, et al. Mechanical behaviour of synthetic surgical meshes: Finite element simulation of the herniated abdominal wall. Acta Biomater 2011;7:3905–13.
10. Otto J, Kaldenhoff E, Kirschner-Hermanns R, Mühl T, Klinge U. Elongation of textile pelvic floor implants under load is related to complete loss of effective porosity, thereby favoring incorporation in scar plates. J Biomed Mater Res A 2014;102:1079–84.